# Journal Pre-proof

Magnetic properties of $Sr_{0.7}R_{0.3}CoO_{3-\delta}$ (R = Tb, Er and Ho) perovskites

V. Cascos, J.L. Martínez, M.T. Fernández-Díaz, J.A. Alonso

PII: S0925-8388(20)32485-3

DOI: https://doi.org/10.1016/j.jallcom.2020.156121

Reference: JALCOM 156121

To appear in: *Journal of Alloys and Compounds*

Received Date: 21 April 2020

Revised Date: 9 June 2020

Accepted Date: 17 June 2020

Please cite this article as: V. Cascos, J.L. Martínez, M.T. Fernández-Díaz, J.A. Alonso, Magnetic properties of $Sr_{0.7}R_{0.3}CoO_{3-\delta}$ (R = Tb, Er and Ho) perovskites, *Journal of Alloys and Compounds* (2020), doi: https://doi.org/10.1016/j.jallcom.2020.156121.

**CRediT author statement:**

**J.A. Alonso** conceived and designed the experiments**; V. Cascos** and **M.T. Fernández-Díaz** performed the experiments; **V. Cascos, J.A. Alonso** and **J.L. Martínez** analyzed the data; **V. Cascos** and **J.A. Alonso** wrote the paper.

# Magnetic properties of $Sr_{0.7}R_{0.3}CoO_{3-\delta}$ (R = Tb, Er and Ho) perovskites

***V. Cascos[a,b*], J.L. Martínez,[a] M.T. Fernández-Díaz,[c] J.A. Alonso[a]***

[a] *Instituto de Ciencia de Materiales de Madrid, C.S.I.C., Cantoblanco E-28049 Spain*

[b] *Departamento de Química Inorgánica, Universidad Complutense de Madrid, E-28040, Madrid, Spain*

[c] *Institut Laue Langevin, BP 156X, Grenoble, F-38042, France*



## ABSTRACT

The $Sr_{0.7}R_{0.3}CoO_{3-\delta}$ (R = Tb, Ho and Er) perovskite derivatives have been previously studied and described as excellent cathode materials for solid-oxide fuel cells (SOFCs) at intermediate temperatures. They were prepared by soft chemistry procedures involving citrates of the different metal ions, followed by thermal treatments in air, and the crystal structure was characterized from neutron powder diffraction (NPD) data in the 300-1100 K temperature range. In this work, these studies have been accompanied with a low-temperature investigation of the magnetic behavior by NPD, in complement with magnetic measurements. For the three members of the series, NPD data unveils a G-type magnetic structure below $T_N$ (~300 K), with a propagation vector k= 0. There is an antiferromagnetic coupling between the two types of Co atoms, defined in the *I4/mmm* space group, with the magnetic moments of Co aligned along the *c* axis of the tetragonal cell. Even at 4 K, the magnetic moments of the rare-earth elements do not participate in the magnetic structure, given their statistical distribution over the Sr positions, and they remain paramagnetic in all the temperature range.

**KEYWORDS:** magnetic structure, cathode for SOFC, $SrCoO_{3-\delta}$, neutron diffraction, antiferromagnetic coupling.

* Corresponding author. Email address: vcascos@icmm.csic.es

## 1. Introduction

Cobalt perovskite oxides exhibit rich magnetic properties due to the unique characteristics possessed by Co ions, which have been exhaustively investigated in the past [1,2]. They exhibit a wide panoply of technological applications, from those derived from their magnetic or electrical behavior (like magnetoresistance or thermoelectricity) to other associated with oxygen diffusion, in solid-oxide fuel cells (SOFC) and membranes for gas separation [3-7]. The magnetic phase diagrams of cobalt perovskites include different phenomenology from paramagnetism (PM), antiferromagnetism (AFM), or ferromagnetism (FM), similar to that presented, for example, by manganites [8-10]. A singularity of Co ions is the variability of the spin states for $Co^{3+}$ and $Co^{4+}$: low spin (S = 0), intermediate spin (S = 1) or high spin (S = 2) for $Co^{3+}$ and (S = 1/2), (S = 3/2) or (S = 5/2) for $Co^{4+}$, with transitions among them that make it difficult the interpretation of the magnetic properties, typically in perovskites $Sr_{1-x}R_xCoO_{3-\delta}$ (R: rare earth) [11-15]. The physical properties of these materials were found to depend on the oxygen content and $R^{3+}/Sr^{2+}$ $Co^{3+}/Co^{4+}$ ratios [16].

In previous works [17-19], $Sr_{0.7}R_{0.3}CoO_{3-\delta}$ (R = Tb, Ho and Er) perovskite materials were evaluated as potential cathodes for solid-oxide fuel cells (SOFCs). The tetragonal crystal structure, defined in the space group *I4/mmm*, was found to contain layers of $CoO_6$ octahedra alternating in a 3D framework with layers of $CoO_4$ tetrahedra, sharing corners. A singular feature was the presence of extra oxygen positions in the tetrahedral layers, with large displacement factors that suggest a large lability and mobility, accounting for their excellent performance as cathodes in SOFC [18]. This work aims at completing the characterization of these perovskites by describing the low-temperature magnetic structures, determined by neutron powder diffraction (NPD), supported with magnetic susceptibility measurements.

## 2. Experimental

$Sr_{0.7}R_{0.3}CoO_{3-\delta}$ (R = Tb, Ho and Er) perovskite-type oxides were obtained by a wet chemistry procedure in which highly reactive precursors were prepared by dissolving stoichiometric amounts of $Tb_4O_7$, $Ho_2O_3$ or $Er_2O_3$, $Sr(NO_3)_2$ and $Co(NO_3)_2{\cdot}6H_2O$ in a citric-acid aqueous solution containing some drops of $HNO_3$. The solutions were slowly evaporated, leading to an organic resin that contains a homogeneous distribution of the involved cations. The formed resins were dried at 120 ºC and decomposed at 600 ºC for 12 h in air. The obtained precursors were then heated at 1100 ºC for 12 h in air. After the thermal treatment, the samples were quenched by opening the furnace door at 1100 ºC and removing the samples to ambient conditions, thus leading to the stabilization of the tetragonal perovskite-oxide phases.

The reaction products were characterized by x-ray diffraction (XRD) for phase identification and to assess phase purity. The characterization was performed using a Bruker-AXS D8 diffractometer (40 kV, 30 mA) in Bragg-Brentano reflection geometry with $CuK_\alpha$ radiation ($\lambda$= 1.5418 Å). NPD data at 298 K were collected for the three materials in the high-resolution powder diffractometer D2B ($\lambda$ = 1.594 Å) at the ILL in Grenoble, within the 2$\theta$ range from 8 to 152º. NPD data at 4 K were collected for $Sr_{0.7}R_{0.3}CoO_{3-\delta}$ (Ho and Er) in a displex unit coupled to the D2B diffractometer, whereas for $Sr_{0.7}Tb_{0.3}CoO_{3-\delta}$ the HRPT diffractometer of the SINQ spallation source (PSI, Switzerland) was utilized, with $\lambda$= 1.494 Å within the 2$\theta$ range from 8 to 145º, coupled to a standard orange cryostat. In all cases, about 2 g of sample were contained in a vanadium can; a time of 3 h was required to collect a full diffraction pattern. The NPD data were analyzed by the Rietveld method [20] with the FULLPROF program [21]. A pseudo-Voigt function was chosen to generate the line shape of the diffraction peaks. The following parameters were refined in the final run: scale factor, background

coefficients, zero-point error, pseudo-Voigt corrected for asymmetry parameters, positional coordinates, magnetic moments and isotropic displacement factors for all the atoms. The coherent scattering lengths for Sr, Er, Ho, Tb, Co and O were 7.02, 7.79, 8.84, 7.38 and 5.805 fm, respectively [22].

The magnetic measurements for the three perovskites were performed in a commercial superconducting quantum interference device (SQUID) magnetometer (Quantum Design MPMS-5S). ZFC (zero field-cooled) and FC (field-cooled) *dc* magnetic susceptibility data were collected in the $4 \leq T \leq 400$ K range under an applied magnetic field of 0.1 T. Isothermal magnetization curves were obtained for magnetic fields going from -5 T to 5 T at $T = 4$ and 300 K.

## 3. Result and discussion

### *3.1. Crystallographic characterization*

$Sr_{0.7}R_{0.3}CoO_{3-\delta}$ (R = Tb, Ho and Er) samples were obtained as well-crystallized powders. The $Sr_{0.7}R_{0.3}CoO_{3-\delta}$ (R = Tb, Ho and Er) crystal structures at 298 and 4 K were refined in the *I*4/*mmm* space group (no. 139), with unit-cell parameters related to the cubic perovskite subcell parameter $a_o$ as $a \approx 2a_o$ and $c \approx 4a_o$. No impurity phases were detected, excepting a tiny amount of $Er_2O_3$ (most intense reflection at 29.6 º 2θ for Er sample) for $Sr_{0.7}Er_{0.3}CoO_{3-\delta}$.

There is no significant evolution of the structural features between both temperatures, besides the expected unit-cell contraction, observed in both *a* and *c* dimensions. The structural model described in refs [18,19] considers that Sr1 and R1 atoms are ordered at two different 4*e* (0, 0, z) sites, whereas (Sr,Ho)2 are distributed at random at 8*g* (0, ½, z) sites. The structure contains two types of Co atoms; Co1 at 8*h* (x, x, 0) and Co2 at 8*f*

(¼,¼,¼) Wyckoff sites. There are four oxygen atoms (O1, O2, O3, O4) located at 16*n* (0, y, z), 16*m* (x, x, z), 8*i* (x, 0, 0) and 8*j* (x, ½, 0) sites, respectively. The refinement of the occupancy factor for all the oxygen atoms shows that O1 and O2 are fully stoichiometric, whereas O3 and O4 exhibit a large sub-stoichiometry (Table 1).

Figures 2.a illustrates the good agreement between observed and calculated neutron diffraction patterns for $Sr_{0.7}R_{0.3}CoO_{3-\delta}$ (R = Tb, Ho and Er) at 298 K and 4 K. The two series of vertical marks for R = Er correspond to the positions of the allowed Bragg reflections for the main perovskite phase and the small $Er_2O_3$ impurity. Table 1 summarizes the unit-cell parameters, atomic positions, occupancies, displacement factors, magnetic moments, selected atomic distances (Å) and reliability factors of $Sr_{0.7}R_{0.3}CoO_{3-\delta}$ (R = Tb, Ho and Er) in the tetragonal *I*4/*mmm* space group (no. 139), from NPD data at 4 and 298 K. The values for 298 K are taken from refs. [18,19] for a better comparison of the data at 4 K. At 298 K [18,19], the refined crystallo-chemical formulae are $Sr_{0.7}Ho_{0.3}CoO_{2.698(1)}$, $Sr_{0.7}Er_{0.3}CoO_{2.782(1)}$ and $Sr_{0.7}Tb_{0.3}CoO_{2.804(1)}$. Taking into account the oxygen vacancies observed at room temperature, and assuming divalent and trivalent oxidation states for Sr and R ions, respectively, a Co valence of $Co^{3.096+}$ for R = Ho, $Co^{3.264+}$ for R = Er and $Co^{3.308+}$ for R = Tb was determined, indicating a mixed valence $Co^{3+}$-$Co^{4+}$. It is important to consider also the impact of the presence of a certain mixed valence $Tb^{3+}$-$Tb^{4+}$ that would lead to a higher oxygen content in this compound. The amount of oxygen vacancies at 4 K does not evolve for R = Ho, and it slightly decreases when cooling the samples for R = Er and Tb, giving crystallographic formulae of $Sr_{0.7}Ho_{0.3}CoO_{2.698(1)}$, $Sr_{0.7}Er_{0.3}CoO_{2.776(1)}$ and $Sr_{0.7}Tb_{0.3}CoO_{2.865(1)}$. Therefore, at this temperature of 4 K, the nominal oxidation state of Co is 3.096+ (Ho), 3.252+ (Er) and 3.430+ (Tb).

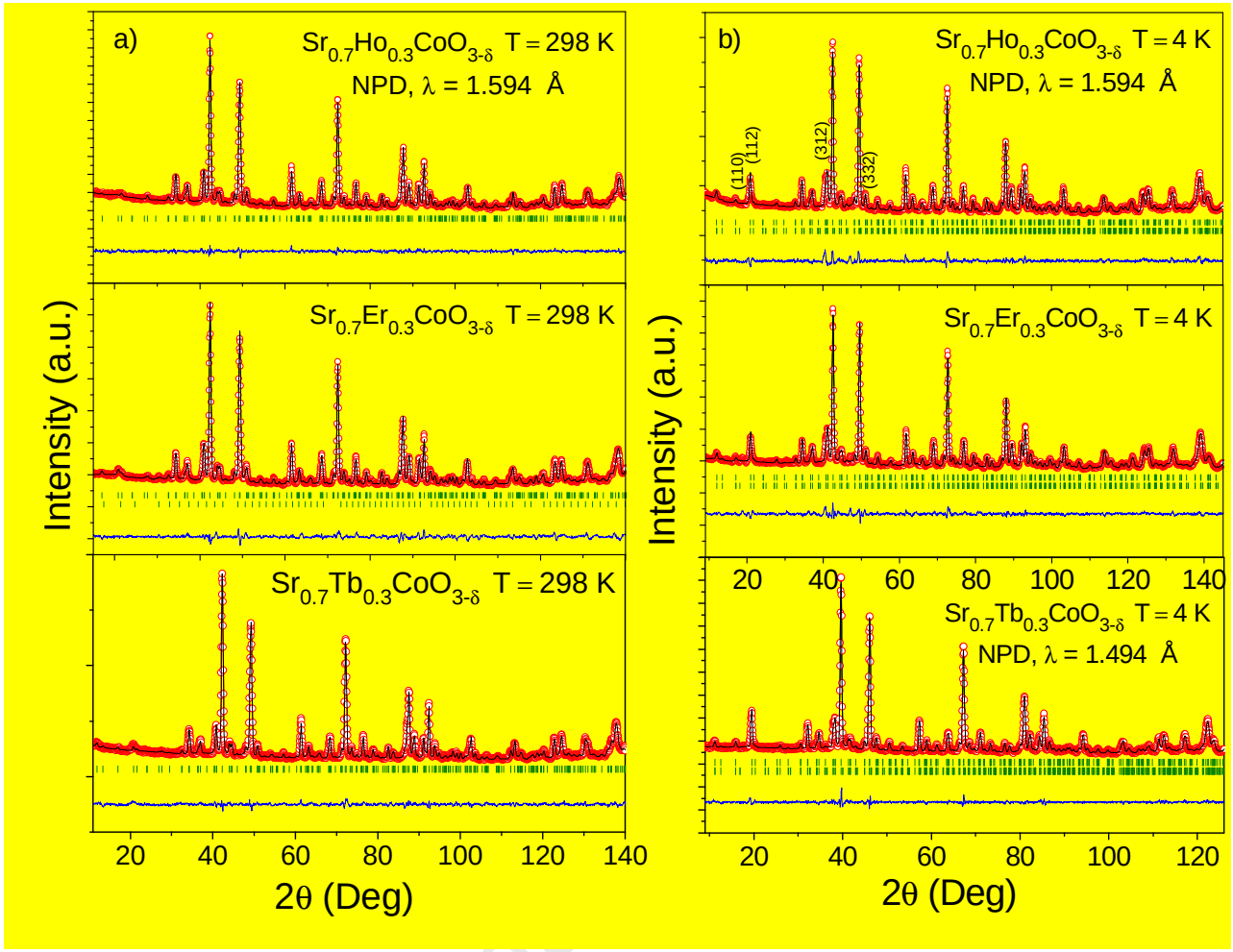


**Fig. 2.** Observed (red circles), calculated (full line), and difference (bottom) NPD Rietveld profiles for $Sr_{0.7}R_{0.3}CoO_{3-\delta}$ (R = Ho, Er and Tb) refined in the tetragonal *I4/mmm* space group. The two series of vertical markers correspond to a) the positions of the allowed Bragg reflections for the crystallographic phase and the minor $Er_2O_3$ impurity for $Sr_{0.7}Er_{0.3}CoO_{3-\delta}$. at 298 K and b) the positions of the allowed Bragg reflections for the crystallographic phase and for the magnetic reflections at 4 K.

It is worth recalling the features of this peculiar superstructure of perovskite [18,19], illustrated in Figure 3. The structure consists of alternating layers of $Co1O_4$ tetrahedra and significantly tilted $Co2O_6$ octahedra. The tetrahedra share two oxygen atoms (O3) in the *ab* plane, additionally containing an extra oxygen atom (O4) with a weak occupancy factor (e.g. 0.632(1) for R= Er, see Table 1)**.** These disordered oxygen atoms increment the coordination of Co1, and they exhibit a large and anisotropic displacement factor (also represented in Figure 3). In fact, Co1 site is effectively five coordinated (Co-O(2) x 2; Co-O3 x 2 and Co-O(4) x 1 allowing for the partial

occupancy) and this should have a smaller average bond length that that of the six-coordinate Co(II) site; as is observed, irrespective of spin states. Along the c axis, the octahedra and tetrahedra are connected by O2 oxygen atoms.

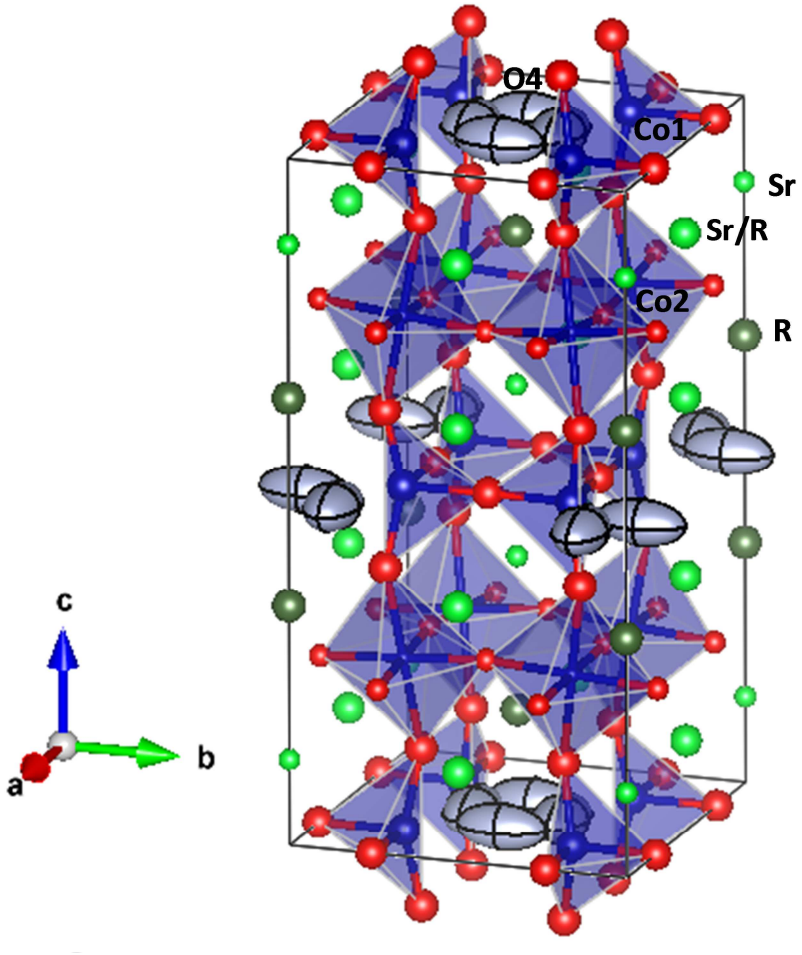


**Fig. 3**. View of the tetragonal crystal structure of $Sr_{0.7}R_{0.3}CoO_{3-\delta}$ (R = Tb, Ho and Er), containing alternating layers of CoO4 tetrahedra and CoO6 octahedra. The tetrahedral layer contains partially occupied O4 oxygen positions, with large anisotropic displacement factors.

In the octahedral layers, the $Co2O_6$ groups exhibit an important axial distortion (see Table 1) with four shorter equatorial distances Co2-O1 around 1.91 Å, and two longer axial distances Co2-O, between 2.047 Å (Tb) and 2.049(5) Å (Er) at 4 K. This suggests the presence of Jahn-Teller-active intermediate-spin $Co^{3+}$ (S=1) in the octahedral Co2 sites, driving an elongation of the axial Co-O bond-lengths. For Co1, the average <Co-O> distances is much smaller, including conspicuously shorter Co1-O2 bonds between

1.845 Å (Tb) and 1.835 Å (Er), suggesting the presence of high-spin $Co^{3+}$ (S= 2) with an admixture of $Co^{4+}$(S= 5/2).

The magnetic structure was determined using the NPD data at 4K for $Sr_{0.7}R_{0.3}CoO_{3-\delta}$ (R = Tb, Ho and Er), where new reflections of magnetic origin appear. Figure 2.b reveals that the magnetic reflections perfectly match with the allowed nuclear reflections, giving rise to a k = 0 propagation vector of the magnetic structure. The Bragg reflections containing a major magnetic contribution at 4 K were indexed in Figure 2.b. The magnetic structure was satisfactorily solved as an antiferromagnetic G-type coupling model between Co1 and Co2 atoms, located at 8*h* and 8*f* positions, respectively. The moments were found to be collinear and (anti) parallel with the c axis. The refined ordered magnetic moments of Co1 and Co2 atoms are found in Table 1; they range between 2.7(3) $\mu_B$ (Tb) and 2.4(1) $\mu_B$ (Er) for Co1 and 1.4(3) $\mu_B$ (Tb) and 1.5(1) $\mu_B$ (Ho) for Co2. These values agree with a high-spin $Co^{3+}$ configuration (S = 2) at the tetrahedral positions whereas an intermediate spin state (S = 1) was found at the octahedral positions, perhaps with a mixture of $Co^{4+}$ (S = 3/2 ). Figure 2.b illustrates the good agreement between the observed and calculated NPD patterns at 4K after the refinement of the crystallographic and magnetic structure for $Sr_{0.7}R_{0.3}CoO_{3-\delta}$ (R = Tb, Ho and Er).

**Table 1.** Unit-cell parameters, atomic positions, occupancies, displacement factors, magnetic moments, selected atomic distances (Å) and reliability factors of $Sr_{0.7}R_{0.3}CoO_{3-\delta}$ (R = Tb, Ho and Er) in the tetragonal *I4/mmm* space group (no. 139), from NPD data at 4 and 298 K. Values at 298 K were taken from refs. [18,19], for a better comparison of the data. The refinements for Tb and Er at 298 K were revised, under the same conditions as the 4 K data.

| ***R*** | ***Tb*** | | ***Ho*** | | ***Er*** | |
|---|---|---|---|---|---|---|
| | ***4 K*** | ***298 K*** | ***4 K*** | ***298 K*** | ***4 K*** | ***298 K*** |
| ***a (Å)*** | *7.6228(2)* | *7.6366(1)* | *7.6076(2)* | *7.6196(1)* | *7.6072(2)* | *7.6241(2)* |
| ***b (Å)*** | *7.6228(2)* | *7.6366(1)* | *7.6076(2)* | *7.6196(1)* | *7.6072(2)* | *7.6241(2)* |
| ***c (Å)*** | *15.2972(6)* | *15.3565(4)* | *15.2505(7)* | *15.3174(4)* | *15.2163(8)* | *15.3046(5)* |
| ***V (Å$^3$)*** | *888.88(4)* | *895.56(3)* | *882.63(5)* | *889.30(3)* | *880.6(6)* | *889.6(4)* |
| ***Sr1 4e (0, 0, z)*** | | | | | | |

| | | | | | | |
|---|---|---|---|---|---|---|
| ***z*** | *0.8782(6)* | *0.8752(4)* | *0.8787(5)* | *0.8794(4)* | *0.8792(6)* | *0.8752(5)* |
| $B_{iso}$ **(Å$^2$)** | *1.1(1)* | *1.2(1)* | *0.9(1)* | *1.26(8)* | *0.4(1)* | *0.7(1)* |
| $f_{occ}$ **Sr** | *1.00* | *1.00* | *1.00* | *1.00* | *1.00* | *1.00* |
| ***R1 4e (0, 0, z)*** | | | | | | |
| ***z*** | *0.3528(4)* | *0.3514(4)* | *0.3514(3)* | *0.3517(2)* | *0.3496(5)* | *0.3486(5)* |
| $B_{iso}$ **(Å$^2$)** | *0.8(1)* | *1.5(1)* | *0.54(9)* | *0.75(7)* | *1.1(2)* | *1.7(1)* |
| $f_{occ}$ **R** | *1.00* | *1.00* | *1.00* | *1.00* | *1.00* | *1.00* |
| ***(Sr,R)2 8g (0, 1/2, z)*** | | | | | | |
| ***z*** | *0.8678(3)* | *0.8696(3)* | *0.8677(3)* | *0.8680(2)* | *0.8670(4)* | *0.8701(3)* |
| $B_{iso}$ **(Å$^2$)** | *0.65(7)* | *1.40(7)* | *0.38(5)* | *0.81(5)* | *0.66(9)* | *1.51(9)* |
| $f_{occ}$ **(Sr/R)** | *0.90/0.10* | *0.90/0.10* | *0.90/0.10* | *0.90/0.10* | *0.90/0.10* | *0.90/0.10* |
| ***Co1 8h (x, x, 0)*** | | | | | | |
| ***x*** | *0.7498(7)* | *0.7525(7)* | *0.7486(8)* | *0.7476(6)* | *0.7488(9)* | *0.7504(9)* |
| $B_{iso}$ **(Å$^2$)** | *1.0(2)* | *1.4(7)* | *0.70(2)* | *1.3(1)* | *0.8(2)* | *1.6(2)* |
| $f_{occ}$ **Co1** | *1.00* | *1.00* | *1.00* | *1.00* | *1.00* | *1.00* |
| ***Co2 8f (¼ , ¼ , ¼ )*** | | | | | | |
| $B_{iso}$ **(Å$^2$)** | *0.4(1)* | *0.8(1)* | *0.3(1)* | *0.7(1)* | *0.5(2)* | *0.4(2)* |
| $f_{occ}$ **Co2** | *1.00* | *1.00* | *1.00* | *1.00* | *1.00* | *1.00* |
| ***O1 16n (0, y, z)*** | | | | | | |
| ***y*** | *0.2461(4)* | *0.2610(4)* | *0.2453(4)* | *0.2452(3)* | *0.2442(5)* | *0.2608(5)* |
| ***z*** | *0.2405(2)* | *0.2417(2)* | *0.2393(2)* | *0.2402(1)* | *0.2398(3)* | *0.2398(3)* |
| $B_{iso}$ **(Å$^2$)** | *0.66(4)* | *0.80(6)* | *0.32(4)* | *0.87(3)* | *0.44(5)* | *0.81(9)* |
| $f_{occ}$ | *1.00* | *0.985(9)* | *1.00* | *1.00* | *1.00* | *1.00* |
| ***O2 16m (x, x, z)*** | | | | | | |
| ***x*** | *0.2834(3)* | *0.2853(2)* | *0.2863(3)* | *0.2859(2)* | *0.2870(3)* | *0.2884(3)* |
| ***z*** | *0.1183(3)* | *0.1163(2)* | *0.1184(3)* | *0.1176(2)* | *0.1179(3)* | *0.1146(3)* |
| $B_{iso}$ **(Å$^2$)** | *2.19(9)* | *2.38(6)* | *1.34(7)* | *1.79(5)* | *1.4(1)* | *1.64(7)* |
| $f_{occ}$ | *1.00* | *1.00* | *1.00* | *1.00* | *1.00* | *1.00* |
| ***O3 8i (x, 0, 0)*** | | | | | | |
| ***x*** | *0.7218(8)* | *0.7557(8)* | *0.7193(7)* | *0.7200(6)* | *0.7224(9)* | *0.7578(8)* |
| $B_{iso}$ **(Å$^2$)** | *1.7(1)* | *2.7(2)* | *1.1(1)* | *1.7(1)* | *0.9(1)* | *1.6(2)* |
| $f_{occ}$ | *0.999(1)* | *0.932(2)* | *0.984(3)* | *0.984(3)* | *0.912(1)* | *0.920(1)* |
| ***O4 8j (x, 1/2, 0)*** | | | | | | |
| ***x*** | *0.353(2)* | *0.357(2)* | *0.390(2)* | *0.383(1)* | *0.392(2)* | *0.371(2)* |
| $B_{eq}$ **(Å$^2$)** | *6.27(1)* | *8.3484* | *4.6(4)* | *5.5(4)* | *3.73(1)* | *6.5895* |
| $\beta_{11}^*$ | - | *518(45)* | - | - | - | *188(35)* |
| $\beta_{22}^*$ | - | *380(39)* | - | - | - | *530(51)* |
| $\beta_{33}^*$ | - | *43(7)* | - | - | - | *33(7)* |
| $f_{occ}$ | *0.731(2)* | *0.706(3)* | *0.412 (3)* | *0.412 (3)* | *0.656(1)* | *0.632(1)* |
| ***Mag. mom.Co1 ($\mu_B$)*** | *2.7(3)* | - | *2.5(1)* | - | *2.4(1)* | - |
| ***Mag.mom.Co2 ($\mu_B$)*** | *1.4(3)* | - | *1.5(1)* | - | *1.5(1)* | - |
| ***Reliability factors*** | | | | | | |
| $\chi^2$ | *1.56* | *2.16* | *2.11* | *1.34* | *2.87* | *3.48* |
| $R_p$**(%)** | *3.38* | *3.09* | *2.71* | *2.23* | *2.56* | *2.87* |
| $R_{wp}$**(%)** | *4.29* | *3.89* | *3.57* | *2.83* | *3.29* | *3.71* |
| $R_{exp}$**(%)** | *3.43* | *2.64* | *2.46* | *2.44* | *1.94* | *1.99* |

| | | | | | | |
|---|---|---|---|---|---|---|
| $R_{Braqq}$(%) | 3.30 | 6.28 | 3.61 | 3.92 | 4.24 | 5.01 |
| $R_{Maq}$(%) | 3.90 | - | 15.60 | - | 13.4 | - |
| **Distances (Å)** | | | | | | |
| **Co1-O2 (x2)** | 1.845(5) | 1.831(1) | 1.844(5) | 1.836(1) | 1.835(5) | 1.803(5) |
| **Co1-O3 (x2)** | 1.920(5) | 1.890(5) | 1.926(6) | 1.935(5) | 1.921(8) | 1.904(8) |
| **Co1-O4(x2)** | 2.095(8) | 2.102(8) | 2.164(9) | 2.133(8) | 2.175(11) | 2.122(9) |
| **Co2-O1(x4)** | 1.9115(4) | 1.9153(2) | 1.9092(3) | 1.9111(2) | 1.9088(4) | 1.9141(4) |
| **Co2-O2(x2)** | 2.047(5) | 2.0890(6) | 2.044(5) | 2.0649(4) | 2.049(5) | 2.113(5) |

*Anisotropic Betas ($x10^4$) $b_{12}=b_{13}=b_{23}=0$

A schematic view of the magnetic structure is shown in Figure 4. The rare-earth moments do not participate in the magnetic structure and remain paramagnetic (disordered) even at this low temperature of 4K, due to the dilution effect with the Sr atoms that are located at the same crystallographic sites, since they are found in a very small proportion (only 30%).

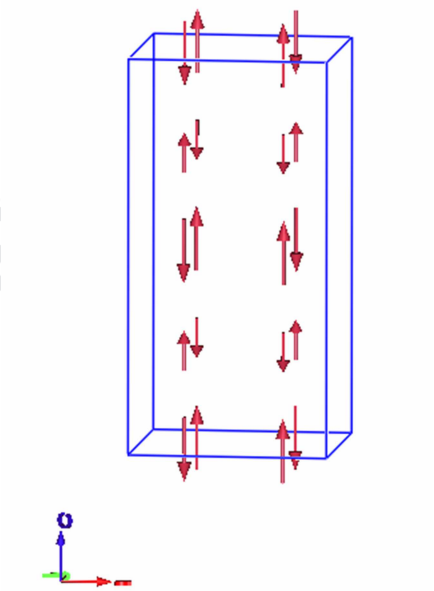


**Fig. 4.** Schematic view of the magnetic structure of $Sr_{0.7}R_{0.3}CoO_{3-\delta}$ (R= Tb, Ho and Er).

*3.2. Magnetic properties*

The thermal evolution of the magnetic susceptibility under an applied field of 0.1 T was measured for $Sr_{0.7}R_{0.3}CoO_{3-\delta}$ (R = Tb, Ho and Er). Figure 5.a represents the *field cooling* curves (FC), showing how the susceptibility increases between 40 and 60 K for the three materials, which is mainly due to the paramagnetic contribution of the rare-earth subcell. This paramagnetic behaviour masks the contributions of the Co atoms. The inset in Figure 5.a shows a zoom of the magnetic susceptibility curves of the $Sr_{0.7}R_{0.3}CoO_{3-\delta}$ (R = Tb, Ho and Er) materials, where an abrupt increase in susceptibility is appreciated between 310 and 320 K for R= Tb, Ho, and a broad maximum with a peak at 290 K for R= Er. These anomalies correspond to a magnetic transition around room temperature; this could be the onset of the antiferromagnetic structure observed for Co spins at 4 K.

Figure 5.b represents the thermal evolution of the reciprocal susceptibility for $Sr_{0.7}R_{0.3}CoO_{3-\delta}$ (R= Tb, Ho and Er). The anomaly previously described for R= Er is also visible in this curve, with a minimum at ~300 K. The reciprocal susceptibility can be described by the Curie-Weiss law above 310 K for $Sr_{0.7}Ho_{0.3}CoO_{3-\delta}$ and $Sr_{0.7}Tb_{0.3}CoO_{3-\delta}$, giving a Weiss temperature, $\theta_{Weiss}$ = -30.4 and -5.2 K, respectively. Negative Weiss temperatures suggest the presence of predominant antiferromagnetic interactions [23]. The observed effective magnetic moments are $\mu_{eff}$ = 6.63 and 6.14 $\mu$B for $Sr_{0.7}Ho_{0.3}CoO_{3-\delta}$ and $Sr_{0.7}Tb_{0.3}CoO_{3-\delta}$. An estimation of the theoretical magnetic moment of $Sr_{0.7}Ho_{0.3}CoO_{3-\delta}$ and $Sr_{0.7}Tb_{0.3}CoO_{3-\delta}$ can be obtained by considering the expression $\mu_{eff} = [0.3(\mu_B R^{3+})^2 + 0.5(\mu_B {}^{HS}Co^{3+})2 + 0.5(\mu_B {}^{IS}Co^{3+})^2]^{1/2}$, where the effective magnetic moments taken for $Ho^{3+}$, $Tb^{3+}$, ${}^{HS}Co^{3+}$ (high spin for the tetrahedral Co1, S = 2) and ${}^{IS}Co^{3+}$ (intermediate spin for octahedral Co2, S = 1) are 10.4, 9.72, 4.90 and 2.83

$\mu_B$, respectively [24-26]. The theoretical effective magnetic moments of $Sr_{0.7}Ho_{0.3}CoO_{3-\delta}$ and $Sr_{0.7}Tb_{0.3}CoO_{3-\delta}$ are 6.96 and 6.66 $\mu$B, which are in reasonable agreement with those observed. In $Sr_{0.7}Er_{0.3}CoO_{3-\delta}$ perovskites, the absence of susceptibility data in the paramagnetic range did not allow a Curie-Weiss fit, which was only performed in the case of the compound doped with Ho and Tb.

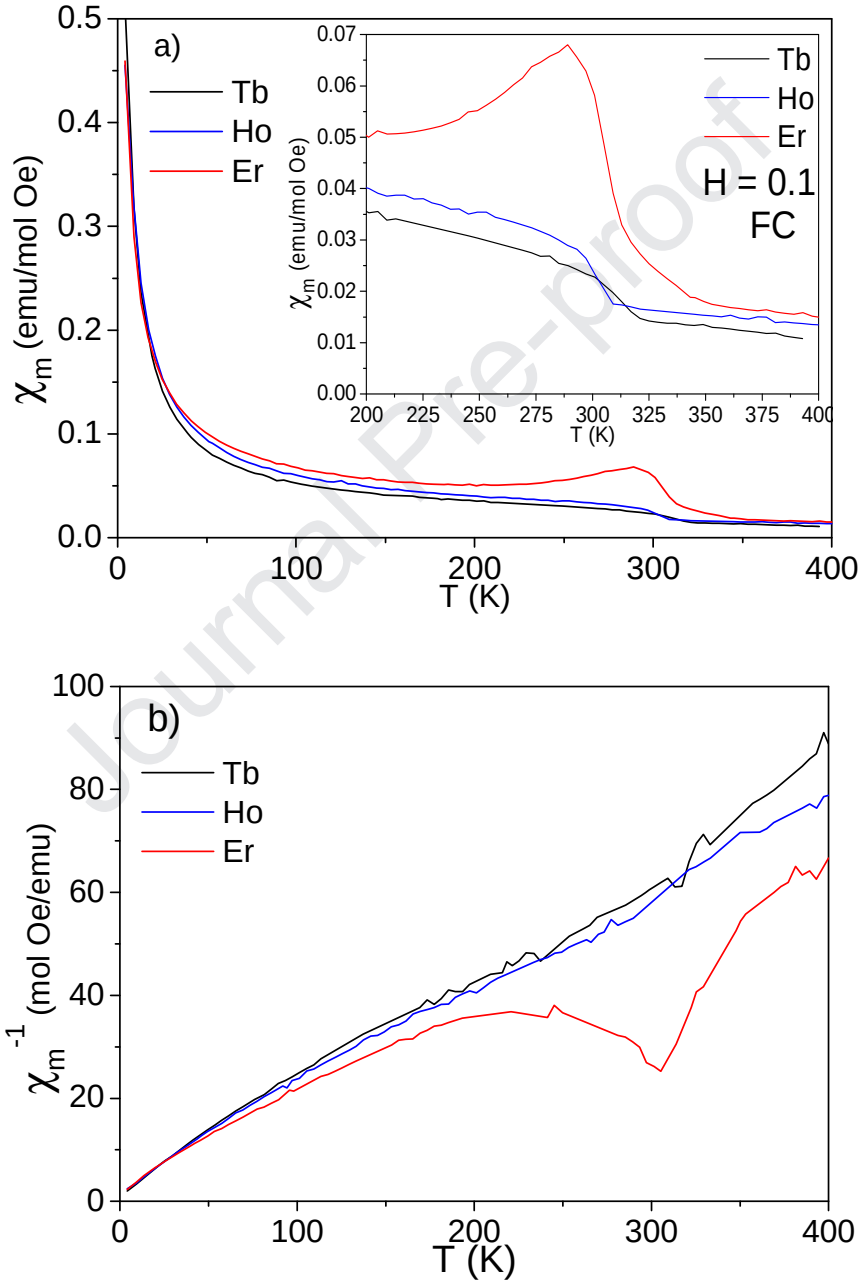


**Fig. 5.** a) Thermal evolution of the magnetic susceptibility (FC curves) for $Sr_{0.7}R_{0.3}CoO_{3-\delta}$ (R= Tb, Ho and Er) at H = 0.1 T. The inset is a zoom of $Sr_{0.7}R_{0.3}CoO_{3-\delta}$ (R= Tb and Ho) between 200 and 400 K. b) Reciprocal susceptibility for $Sr_{0.7}R_{0.3}CoO_{3-\delta}$ (R= Tb, Ho and Er).

Although a magnetic order temperature is suggested slightly above RT (310 K) by the magnetic susceptibility data, no measurable magnetic contribution to the scattering is appreciated in the NPD diagrams at room temperature (Figure 2.a), since the magnetic structures may still exhibit a short-range correlation, or perhaps, the ordered magnetic moments are very weak. No diffuse scattering was observed, neither broadening of the peaks in the low-angle reflections. The background was correctly fitted by interpolation between points devoid of reflections.

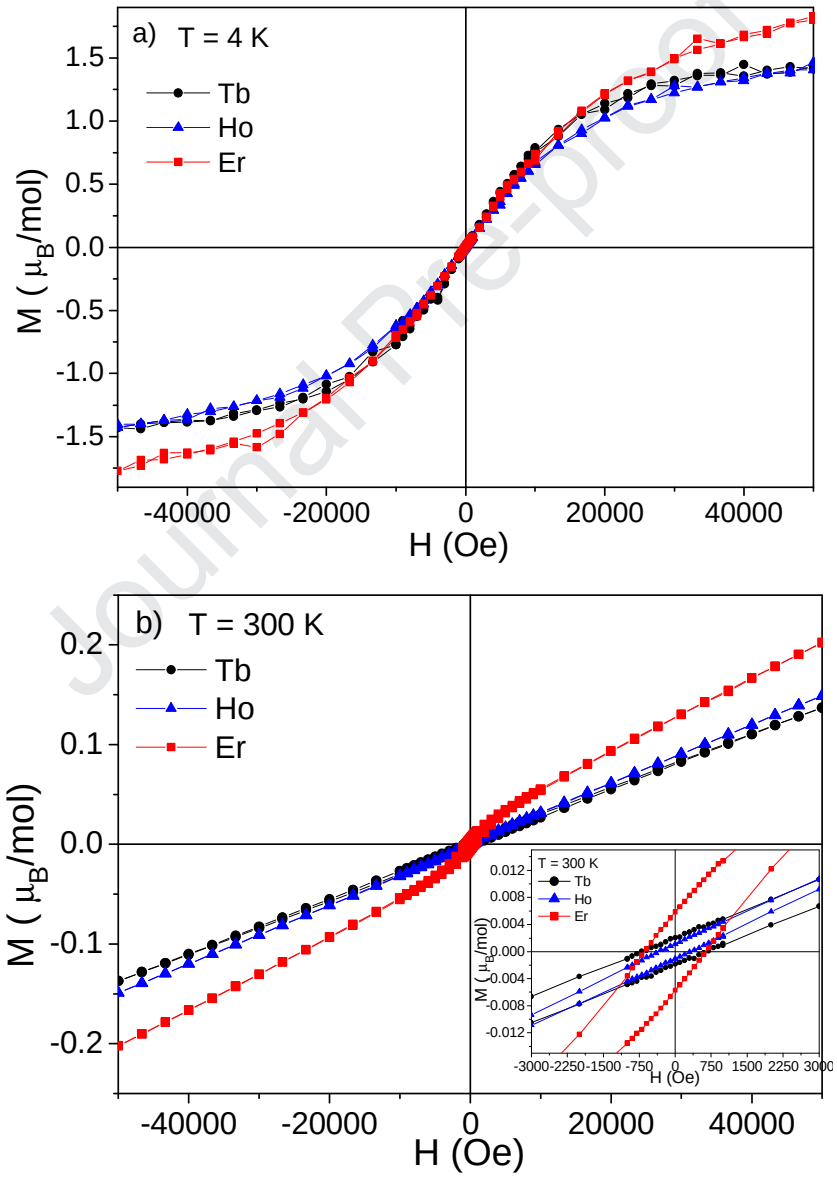


**Fig. 6.** a) Magnetization vs magnetic field isotherms at T = 4 K for $Sr_{0.7}R_{0.3}CoO_{3-\delta}$ (R= Tb, Ho and Er). b) Magnetization *vs* magnetic field isotherms at T = 300 K for $Sr_{0.7}R_{0.3}CoO_{3-\delta}$ (R= Tb, Ho and Er). The inset shows a zoom of the magnetization at low applied fields.

Figures 6.a and 6.b show the isothermal magnetization curves *vs* magnetic field measured at 4 and 300 K for the three perovskites. No hysteresis or saturation loops were observed at high applied fields (5T) at 4 K, thus excluding the presence of ferromagnetic interactions in $Sr_{0.7}R_{0.3}CoO_{3-\delta}$ (R= Tb, Ho and Er); the observed magnetization is due to the polarization of the paramagnetic moments of the rare-earth cations when an external magnetic field is applied. Values between 1.4 and 1.8 $\mu_{B/mol}$ are reached for Ho, Tb and Er with H = 5 T at 4 K. A coercive field is not observed at this temperature.

At 300 K, a linear M *vs* H behavior with very narrow hysteresis loops is shown at low magnetic fields, as shown the inset in Figure 6.b. These narrow hysteresis loops exhibit a remnant magnetization of Mr = 0.0011, 0.0021 and 0.0059 $\mu_{B/mol}$ and a coercive field $H_{Co}$ = 345, 700 y 644 Oe for $Sr_{0.7}Ho_{0.3}CoO_{3-\delta,}$ $Sr_{0.7}Tb_{0.3}CoO_{3-\delta}$ y $Sr_{0.7}Er_{0.3}CoO_{3-\delta,}$ respectively. These values suggest the presence of weak ferromagnetism correlations, perhaps due to a subtle canting of the Co moments upon the magnetic transitions identified above room temperature (inset of Fig. 5a) [27,23], which prevented an accurate Curie Weiss fit. Magnetization values at high fields are illustrated in Figure 6.b in the isotherms at 300 K. Maximum values of 0.137, 0.148 and 0.202 $\mu_{B/mol}$ are reached for Ho, Tb and Er with H = 5 T. As temperature is decreasing, the rare-earth atoms start to be polarized, and a net magnetization is observed. This masks the antiferromagnetism from cobalt atoms and a possible subtle canting of the Co moments, not observed by neutron diffraction.

## 4. Conclusions

In this work, the magnetic structures of the $Sr_{0.7}R_{0.3}CoO_{3-\delta}$ (R= Tb, Ho and Er) perovskites, previously evaluated as cathode materials in Refs. [17-19], have been determined. At room temperature, these oxides exhibit a tetragonal perovskite-like superstructure defined in the *I4/mmm* space group, containing two types of Co environments, in octahedral (Co1) and tetrahedral (Co2) oxygen coordination. A NPD study at 4 K was performed to determine the magnetic order of these materials. The magnetic structure was solved with a G-type antiferromagnetic coupling model between Co1 and Co2 moments, aligned along the c axis of the tetragonal cell. The Co1 ordered moments are considerably higher than those found at the octahedral Co2 positions, which is understood as a function of the occurrence of different spin states of Co ions in both coordination sites. The magnetic susceptibility curves show subtle magnetic transition near room temperature (~300 K) for the three compounds. The paramagnetic contribution of the rare-earth moments predominates below 40-60 K depending on the compound, masking the behavior of the Co magnetic sublattice. The Curie-Weiss law was verified only for the $Sr_{0.7}Ho_{0.3}CoO_{3-\delta}$ and $Sr_{0.7}Tb_{0.3}CoO_{3-\delta}$ compounds in the 320-400 K temperature range; the paramagnetic moment is compatible with an as mixture of $^{HS}Co^{3+}$ (high spin for the tetrahedral Co1, S = 2) and $^{IS}Co^{3+}$ (intermediate spin for octahedral Co2, S = 1). For Er material, the Curie-Weiss law was not verified in the available temperature range.

## Acknowledgements

We thank the financial support of the Spanish Ministry of Industry and Competitiveness to the project MAT2017-84496-R. We thank the PSI and the ILL for making all

facilities available. V.C. thanks the Community of Madrid for granting “Atracción de Talento program” fellowship, 2019-T2/IND-13483.

**References**

[1] B. Raveau, M. Seikh, Chapter 3 - Magnetic and Physical Properties of Cobalt Perovskites, Handbook of Magnetic Materials 23 (2015) 161-289.

[2] J.B. Goodenough et al. Landolt-Börnstein: Numerical Data and Functional Relationships in Science and Technology. Vol. 4, Magnetic and Other Properties of Oxides and Related Compounds, Springer, New York, 1970.

[3] F.C. Chou, J.H. Cho, Y.S. Lee, Magnetic susceptibility study of hydrated and nonhydrated $Na_xCoO_2{\cdot}yH_2O$ single crystals. Phys. Rev. B 70 (2004) 144526. https://doi.org/10.1103/PhysRevB.70.144526

[4] S. Roy, I.S. Dubenko, M. Khan, E.M. Candon, N. Ali, Magnetic properties of perovskite-derived air-synthesized $RBaCo_2O_{5+\delta}$ (R=La and Ho) compounds, Phys. Rev. B 71 (2005) 024419. https://doi.org/10.1103/PhysRevB.71.024419.

[5] R. Mahendiran, P. Schiffer, Double magnetic transition in $Pr_{0.5}Sr_{0.5}CoO_3$, Phys. Rev. B. 68 (2003) 024427. https://doi.org/10.1103/PhysRevB.68.024427

[6] R.H.E. van Doorn, A.J. Burggraaf, Structural aspects of the ionic conductivity of $La_{1-x}Sr_xCoO_{3-\delta}$, Solid State Ionics. 128 (2000) 65-78. https://doi.org/10.1016/S0167-2738(99)00282-9.

[7] V.V. Kharton, A.A. Yaremchenko, A.V. Kovalevsky, A.P. Viskup, E.N. Naumovich, P.F. Kerko, Perovskite-type oxides for high-temperature oxygen separation membranes, J. Membr. Sci. 163 (1999) 307-317. https://doi.org/10.1016/S0376-7388(99)00172-6.

[8] G.H. Jonker, J.H. van Santen, Magnetic compounds with perovskite structure III. ferromagnetic compounds of cobalt, Physica 19 (1953) 120-130. https://doi.org/10.1016/S0031-8914(53)80011-X.

[9] V.G. Bhide, D.S. Rajoria, C.N.R. Rao, G. Rama Rao, V.G. Jadhao, Itinerant-electron ferromagnetism in $La_{1-x}Sr_xCoO_3$: A Mössbauer study, Phys. Rev. B 12 (1975) 2832. https://doi.org/10.1103/PhysRevB.12.2832.

[10] M.A. Senaris-Rodriguez, J.B. Goodenough, Magnetic and Transport Properties of the System $La_{1-x}Sr_xCoO_{3-\delta}$ ($0 < x \leq 0.50$), J. Solid State Chem. 118 (1995) 323-336. https://doi.org/10.1006/jssc.1995.1351.

[11] R. Mahendiran, A.K. Raychaudhuri, Magnetoresistance of the spin-state-transition compound $La_{1-x}Sr_xCoO_3$, Phys. Rev. B. 54 (1996) 16044. https://doi.org/10.1103/PhysRevB.54.16044.

[12] S. Mukherjee, R. Ranganathan, P.S. Anilkumar, P.A. Joy, Static and dynamic response of cluster glass in $La_{0.5}Sr_{0.5}CoO_3$ Phys. Rev. B. 54 (1996) 9267. https://doi.org/10.1103/PhysRevB.54.9267.

[13] D.N.H. Nam, K. Jonason, P. Nordblad, N.N. Khiem, N.X. Phuc, Coexistence of ferromagnetic and glassy behavior in the $La_{0.5}Sr_{0.5}CoO_3$ perovskite compound, Phys. Rev. B 59 (1999) 4189. https://doi.org/10.1103/PhysRevB.59.4189.

[14] R. Caciuffo, D. Rinaldi, G. Barucca, J. Mira, J. Rivas, M.A. Señarís-Rodríguez, P.G. Radaelli, D. Fiorani, J.B. Goodenough, Structural details and magnetic order of $La_{1-x}Sr_xCoO_3$ (x<~0.3), Phys. Rev. B. 59 (1999) 1068. https://doi.org/10.1103/PhysRevB.59.1068.

[15] J. Wu, C. Leighton, Glassy ferromagnetism and magnetic phase separation in $La_{1-x}Sr_xCoO_3$, Phys. Rev. B. 67 (2003) 174408. https://doi.org/10.1103/PhysRevB.67.174408.

[16] M.A. Senaris-Rodriguez, M.P. Breijo, S. Castro, C. Rey, M. Sánchez, R.D. Sánchez, et al. Peculiarities in the electrical and magnetic properties of cobalt perovskites $Ln_{1-x}M_xCoO_3$ ($Ln^{3+}$: $La^{3+}$, $M^{2+}$: $Ca^{2+}$, $Sr^{2+}$, $Ba^{2+}$; $Ln^{3+}$: $Nd^{3+}$, $M^{2+}$: $Sr^{2+}$). Int. J. Inorg. Mater. 1 (1999) 281-287. https://doi.org/10.1016/S1466-6049(99)00042-2.

[17] T. Liu, Y. Li, J.B. Goodenough, $Sr_{0.7}Ho_{0.3}CoO_{3-\delta}$ as a Potential Cathode Material for Intermediate-Temperature Solid Oxide Fuel Cells. J. Power Sources 199 (2012) 161 −164. https://doi.org/10.1016/j.jpowsour.2011.10.028.

[18] V. Cascos, R. Martínez-Coronado, J.A. Alonso, M.T. Fernández-Díaz, Visualization by neutron diffraction of 2D oxygen diffusion in the $Sr_{0.7}Ho_{0.3}CoO_{3-\delta}$ cathode for solid-oxide fuel cells, ACS Appl. Mater. Interfaces 6 (2014) 9194-9200. https://doi.org/10.1021/am501297z.

[19] V. Cascos, A. Aguadero, G. Harrington, M.T. Fernandez-Díaz, J.A. Alonso, Design of $Sr_{0.7}R_{0.3}CoO_{3-\delta}$ (R = Tb and Er) Perovskites Performing as Cathode Materials in Solid Oxide Fuel Cells, J. Electrochem. Soc, 164 (2017) F3019-F3027. https://doi.org/10.1149/2.0031710jes.

[20] H.M.A Rietveld, Profile refinement method for nuclear and magnetic structures, J Appl Crystallogr. 2 (1969) 65-71. https://doi.org/10.1107/S0021889869006558.

[21] J. Rodríguez-Carvajal, Recent advances in magnetic structure determination by neutron powder diffraction, Phys B. 192 (1993) 55-69. https://doi.org/10.1016/0921-4526(93)90108-I.

[22] R.D. Shannon, Revised effective ionic radii and systematic studies of interatomic distances in halides and chalcogenides, Acta Crystallogr. A 32 (1976) 751–767. https://doi.org/10.1107/S0567739476001551.

[23] A. Hassen, A.I. Ali, B.J. Kim, Y.S. Wu, S.H. Park. Structural, magnetic, and electric properties of $Dy_{1-x}Sr_xCoO_{3-\delta}$ ($0.65 \leq x \leq 0.90$), Journal of applied physics 102 (2007) 123905. https://doi.org/10.1063/1.2822459

[24] E.M. Larsen, Elementos de transición. Ed. Reverté, s.a. Spain, 1970, Pg. 25.

[25] A.R. West, Basic Solid State Chemistry, Ed. John Wiley & Sons, London, 1999, Pg 347.

[26] N.O. Golosova, D.P. Kozlenko, L.S. Dubrovinsky, O.A. Drozhzhin, S. Ya. Istomin, B.N. Savenko. Spin state and magnetic transformations in $Sr_{0.7}Y_{0.3}CoO_{2.62}$ at high pressures. Phys. Rev. B, 79 (2009) 104431. https://doi.org/10.1103/PhysRevB.79.104431.

[27] D.J. Goossens, K.F. Wilson, M. James, A.J. Studer, X.L. Wang, Structural and magnetic properties of $Y_{0.33}Sr_{0.67}CoO_{2.79}$, Phys. Rev. B, 69 (2004) 134411. https://doi.org/10.1103/PhysRevB.69.134411.

- $Sr_{0.7}R_{0.3}CoO_{3-\delta}$ (R = Ho, Tb and Er) perovskites are excellent cathodes in SOFC.

- The magnetic order and magentic structure of these materials are identified by neutron diffraction at 4K.

- Subtle magnetic transition near room temperature (~300 K) for the three compounds is shown.

- The Curie-Weiss law is verified for the compounds in the 320-400 K temperature range.

**Declaration of interests**

☒ The authors declare that they have no known competing financial interests or personal relationships that could have appeared to influence the work reported in this paper.

☐The authors declare the following financial interests/personal relationships which may be considered as potential competing interests: